REPORTS

COMPOSITES

Layered and scrolled nanocomposites with aligned semi-infinite graphene inclusions at the platelet limit

Pingwei Liu,[1] Zhong Jin,[1,2] Georgios Katsukis,[1] Lee William Drahushuk,[1] Steven Shimizu,[1] Chih-Jen Shih,[1] Eric D. Wetzel,[3] Joshua K. Taggart-Scarff,[3] Bo Qing,[4] Krystyn J. Van Vliet,[4,5] Richard Li,[6] Brian L. Wardle,[6] Michael S. Strano[1]*

Two-dimensional (2D) materials can uniquely span the physical dimensions of a surrounding composite matrix in the limit of maximum reinforcement. However, the alignment and assembly of continuous 2D components at high volume fraction remain challenging. We use a stacking and folding method to generate aligned graphene/polycarbonate composites with as many as 320 parallel layers spanning 0.032 to 0.11 millimeters in thickness that significantly increases the effective elastic modulus and strength at exceptionally low volume fractions of only 0.082%. An analogous transverse shear scrolling method generates Archimedean spiral fibers that demonstrate exotic, telescoping elongation at break of 110%, or 30 times greater than Kevlar. Both composites retain anisotropic electrical conduction along the graphene planar axis and transparency. These composites promise substantial mechanical reinforcement, electrical, and optical properties at highly reduced volume fraction.

The concept of nanocomposites is motivated by the observation that filler particles can stiffen and strengthen otherwise softer materials such as polymers to form lightweight, sturdy composites. Eshelby (*1*) first demonstrated this possibility mathematically for ellipsoidal "inclusions" in a solid. In practice, however, it has proven exceedingly difficult to insert closely spaced but distinctly separated nanoparticles within a material, a fundamental requirement for strengthening it. For anisotropic nanoparticles, such as platelets, nanofibers, or nanotubes (*2*, *3*), mechanical reinforcement can occur at very low volume fractions of the added filler, because the particles can align along preferential axes of strain (*4*–*6*). For a platelet filler such as graphene or other two-dimensional (2D) materials, however, a unique limit can be realized as the aspect ratio, a, of the aligned plates approaches infinity. A closely spaced stack of aligned, semi-infinite plates of nanometer or atomic thickness approaches a limit of maximal mechanical reinforcement at minimal platelet addition per mass of material. It has only recently become possible to test this $a \rightarrow \infty$ limit with the development of chemical vapor deposition (CVD) methods of creating single-unit cell- or atom-thickness films, such as graphene (*7*, *8*) and other 2D materials (*9*) that can span the physical dimensions of a composite large enough for testing. In this work, we introduce two fabrication methods that can take a thin layer of molecular thickness and construct large composite stacks that scale exponentially with the number of processing steps. An analogous shear scrolling method creates Archimedean scroll fibers from single layers with similar scaling. The methods produce materials that demonstrate the $a \rightarrow \infty$ limit while combining electrical and optical properties at minimal volume fraction of the filler.

The planar stacking method generates a thickness that exponentially scales with each successive quadrant fold or segmentation, j, as 4^j. Further hot-pressing promotes the interlayer integration (Fig. 1A). Replicating the process j times generates a nanocomposite of $i \times 4^j$ layers and a lateral dimension of $W/4^j$, where i is the initial stacking or number of layers and W is the initial width of the i-layer composite (Figs. 1, B to D). We use polycarbonate (PC) as the polymer matrix due to its transparency and mechanical strength, creating bulk composites from CVD monolayer, polycrystalline graphene (*10*) (Fig. 2A) with layer numbers of 8 to 320 and volume fractions (V_Gs) of 0.003 to 0.185% (figs. S1 and S2 and table S1). The graphene layers appear intact upon this processing because the size of the translucent area containing graphene exhibits little change after each pressing step. Raman spectroscopy (Fig. 2, B and C, and fig. S3) confirms that the absolute intensity of the graphene 2D peak (I_{2D}) decreases with increasing layer number, approximately following the Lambert-Beer law (fig. S3C and supplementary text 1).

$$-\lg\left(I_{2D}/n\right) = kn + c \quad (1)$$

The equation is verified by well-fit least-squares regression of these data for graphene/polycarbonate (G/PC) composites of $V_G \approx 0.030\%$ and of $V_G \approx 0.009\%$, each ranging from 1 to 144 layers (Fig. 2C). The differences between the two fitted curves are very small due to the very low extinction coefficient (≈ 0) of the highly transparent PC layer. The composites have high optical transmittance of 90% at 9 layers and 58% at 36 layers, following the Lambert-Beer law (fig. S4), corresponding to a transmittance of 98% per layer, in agreement with the known visible light transmittance of monolayer graphene (*11*). We also found an alternate route to stacked, planar composites by monomer impregnation and in situ polymerization within expanded graphite derived from the thermal treatment of iodine chloride–intercalated highly ordered pyrolytic graphite (*12*), achieving up to $V_G \approx 0.60\%$ (fig. S5). However, the quality and control of layer spacing for the resulting composite was found to be lower than the 4^j method (fig. S5E).

We also use an analogous stacking procedure to create Archimedean spiral fibers (Fig. 1, E to I, and figs. S6 to S8). A transverse shear force scrolls a single G/PC film (2.0 × 2.2 cm) into a fiber (Fig. 1E) of diameter 105 ± 2 μm (fiber 1) measured optically (figs. S6 and S7) and 160 ± 4 μm (fiber 2) (Fig. 1F and figs. S6 and S8). The layer spacing of 180 and 410 nm, respectively, induces an observable multilayer thin-film interference in Fig. 1F (and fig. S6, B and C), respectively. The fiber axial cross section has a deformed spiral structure (Fig. 1, G to I, and fig. S9). Both methods can control the resulting V_G over three orders of magnitude from 0.003 to 2.55% (table S1).

Despite having vanishingly small V_Gs, such aligned composites demonstrate substantial increases in both the uniaxial tensile storage moduli (E') and loss moduli (E'') from dynamic mechanical analysis (DMA) (Fig. 3, A and B). Two 4^j planar samples with $V_G \approx 0.082$ and 0.185%, respectively, both at 40 layers, have significantly higher E' than pure PC controls (Fig. 3A), with E'/E'_{PC} = 2.36/2.04 (GPa/GPa) and 2.70/2.04 at 30°C, for example, or an increased stiffness ΔE up to 0.66 GPa or 30%. We estimate the effective elastic modulus of the component graphene layers as 360 GPa with the rule of mixtures, agreeing with reported values of 210 to 510 GPa for CVDGs with ripples (*13*, *14*). Uniaxial tension (fig. S10) and microindentation results (fig. S11) demonstrate similar elastic modulus increase with a linear dependence on V_G. For comparison, a minimum of $2\% < V_G < 5\%$, 10 times more than 4^j composites, is required to achieve comparable stiffness of PC nanocomposites in the limit of 3D random orientation for graphene oxide (GO) or derivatives with typical aspect ratios a = 20 to 50 (*15*–*18*) (Fig. 3C). Nanoplatelets with smaller a values contribute less to reinforcement (fig. S12); GOx (or derivatives)

[1]Department of Chemical Engineering, Massachusetts Institute of Technology, Cambridge, MA 02139, USA. [2]Key Laboratory of Mesoscopic Chemistry of MOE and Collaborative Innovation Center of Chemistry for Life Sciences, School of Chemistry and Chemical Engineering, Nanjing University, Nanjing, Jiangsu 210093, China. [3]U.S. Army Research Laboratory, Aberdeen Proving Ground, MD 21005-5069, USA. [4]Department of Biological Engineering, Massachusetts Institute of Technology, Cambridge, MA 02139, USA. [5]Department of Materials Science and Engineering, Massachusetts Institute of Technology, Cambridge, MA 02139, USA. [6]Department of Aeronautics and Astronautics, Massachusetts Institute of Technology, Cambridge, MA 02139, USA.
*Corresponding author. Email: strano@mit.edu

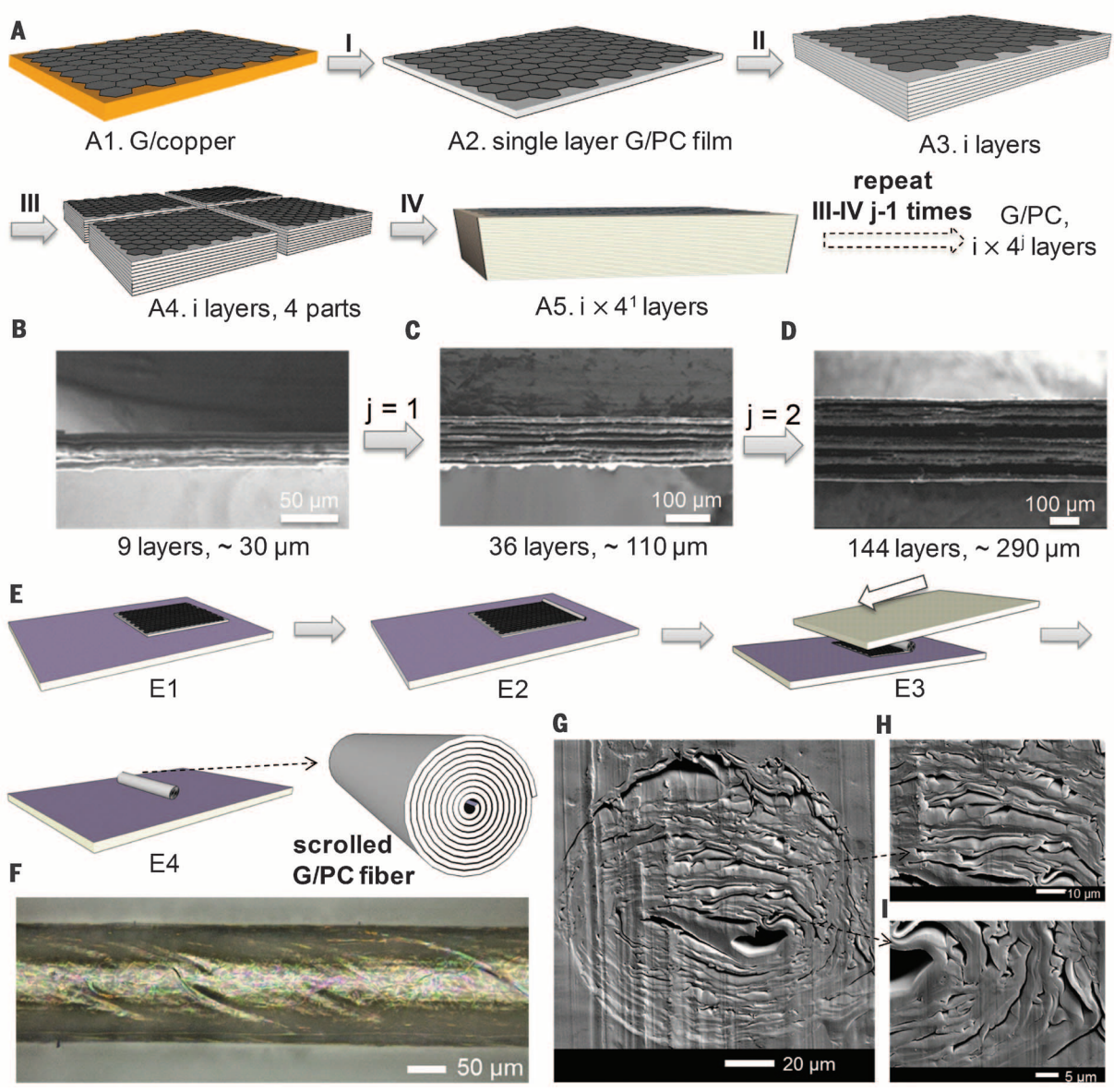

Fig. 1. Fabrication of G/PC composites with aligned, semi-infinite CVD graphene. (**A**) A 4^j stacking method for planar 4^j composites: (I) spin-coating of PC solution and etching out copper, (II) stacking i layers of G/PC films, (III) cutting/folding, and (IV) stacking and hot-pressing at 37 MPa and 155°C. (**B** to **D**) SEM images of the planar composites with i = 9 (3570 nm/layer, $V_G \approx 0.009\%$), j = 1, and j = 2, respectively. (**E**) The transverse shear method for scrolled nanocomposite fiber. (E1) A single layer of G/PC film supported on Si/SiO_2 substrate. (E2) The supported film with folds at one end created by a glass capillary. (E3) The scrolling of the film by the transverse shear force exerted by the two Si/SiO_2 wafers. (E4) A scrolled fiber with Archimedean spiral pattern in the cross-section plane. (**F**) Optical microscope image of fiber 2 with diameter (d) = 160 ± 4 μm. (**G** to **I**) SEM images of fiber 2 with d = 131 ± 3 μm in the cross-section plane. Scale bars are 20, 10, and 5 μm, respectively.

with multilayer structures generally have poor interlayer bonding (*19*, *20*), which further minimizes the reinforcement. The atomic thinness of monolayer CVDG and its near-infinite a maximize this reinforcement (Fig. 3C).

We also verified that the PC matrix of our composite is not itself stiffening, evidenced by the reduction of the glass transition temperature (T_g) from 151.3° to 141.8°C at higher V_Gs (fig. S13) and no detectable increase in crystallinity of the PC (Fig. 3A). The reinforcement then comes from the direct load transfer to graphene filler itself (*21*), distinguishing it from cases where the inclusion (e.g., GO) stiffens the polymer matrix and increases T_g by restricting polymer-chain mobility near the polymer-inclusion interface (*19*, *22*) (fig. S14 and supplementary text 5). To date, we have demonstrated composites with V_G as high as 0.185%, but the 4^j and shear scrolling methods allow one to reach as high as 2.5% (table S1), translating to ΔE (or $\Delta E'$) = 9.0 to 20.6 GPa (Fig. 3C). Planar 4^j samples at $V_G \approx 0.185\%$ also show higher E'' peak values (0.50 GPa) compared with those at $V_G \approx$ 0.082% (0.40 GPa) and the PC control (0.26 GPa) (Fig. 3A). These samples possess an enhanced energy dissipation mechanism from in-plane translation and frictional sliding at the layer interfaces (fig. S10A) (*23*). Both E' and E'' increase with V_G, promising materials of stiffness and damping exceeding that of the matrix polymer at negligible increases in weight (*24*).

The spiral fibers also demonstrate interesting mechanical properties. Two Archimedean scroll fibers—fiber 1 ($V_G \approx 0.185\%$) and fiber 2 (0.082%)—exhibit higher E' of 2.07 and 1.62 GPa, respectively, compared with PC controls at 1.14 GPa over 30° to 150°C (Fig. 3B). However, the stiffness of these scroll fiber composites was generally lower than that of the planar 4^j composites. The scrolled structures of the fibers demonstrate a telescoping compliance mechanism (Fig. 3D, I) that involves internal axial rotation in addition

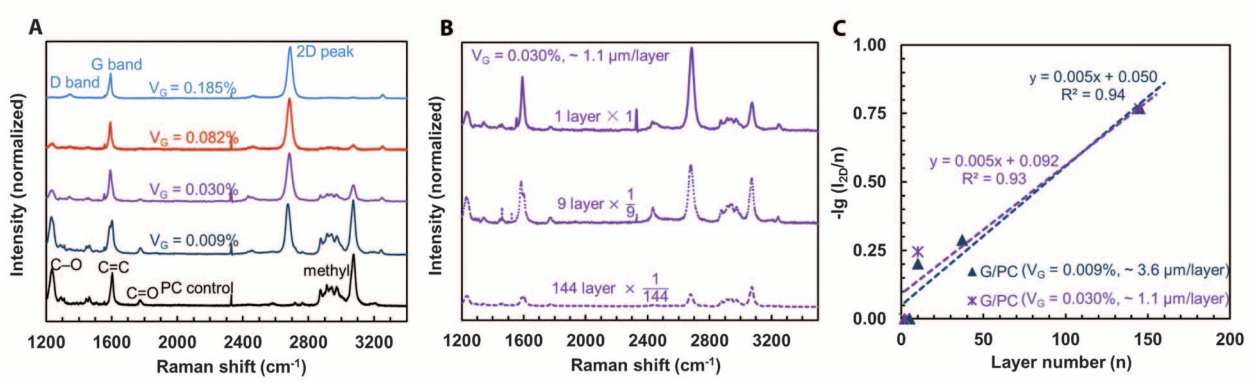

Fig. 2. Raman spectroscopy study of G/PC composites. (**A**) Raman spectra of G/PC composites (1 layer) and PC matrix control. The intensity ratio of 2D peak to G peak (I_{2D}/I_G) = 2.1 indicates the monolayer nature of graphene (*8*, *10*). A small D band at 1350 cm^{-1} illustrates the polycrystalline nature of CVDG (*10*). The resonance-enhanced graphene Raman cross section is 18,000 times as large as PC (fig. S4A). (**B**) Raman spectra of G/PC composites ($V_G \approx 0.030\%$) with layer number (n) of 1, 9, and 144; the spectroscopy intensity was normalized by n. (**C**) Plots of $-\lg(I_{2D}/n)$ against n for G/PC composites with $V_G \approx 0.009$ and 0.030%.

Fig. 3. Mechanical characterization of G/PC planar and scrolled fiber nanocomposites. (**A**) The storage modulus (E') and loss modulus (E'') versus temperature curves of two 40-layer planar composites with $V_G \approx 0.185$ and 0.082%, and PC matrix control (strain amplitude = 0.34%; frequency = 1 Hz). (**B**) E' and E'' versus temperature curves of fiber 1 ($V_G \approx 0.185\%$), fiber 2 (0.082%), control-1 and control-2 (with similar scroll structure). (**C**) A comparison of the elastic modulus increase (ΔE and $\Delta E'$) with respect to the PC matrix, against V_G of planar composites and scrolled fibers with reported data of various G/PC composites (*15*–*18*). The dashed lines are predicted by Mori-Tanaka theory (supplementary text 2). (**D**) The ideal telescoping mechanism (I). In practice, deformation occurs internally in the bulk of the fiber and not near the gripped fiber ends; the optical image of the scrolled fiber 2 in tensile with $d = 120 \pm 2$ μm at 60% strain (II) and at break (III and IV); SEM image of scrolled fiber (control-1) at break (V), demonstrating layer separations during failure. (**E**) True stress-strain responses of two composite fibers and their PC control fibers with similar scroll structures.

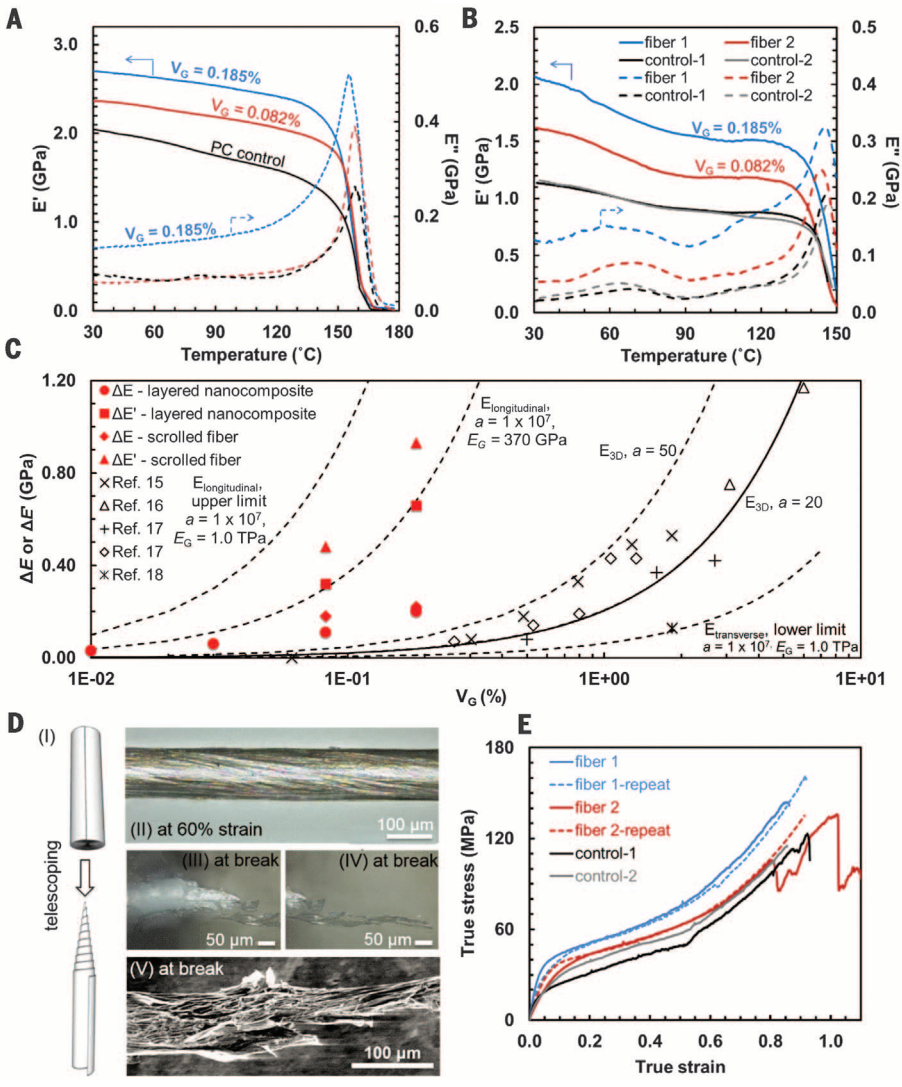

to the interlayer translation shown in the planar 4^j systems (fig. S10A). These fibers still exhibited measurable increases in stiffness $\Delta E'$ of 0.38 and 0.93 GPa, however, and larger effective E_G of the CVDG at 500 GPa. This telescoping compliance may necessarily reduce in-plane ripples to realize this increase. The scroll fibers also helically telescope in tension, necessarily reducing the diameter and densifying the structure uniformly (Fig. 3D, II, and fig. S15A). Axial rotation, in addition to translation, increases the path length per unit axial strain, hence increasing the E'' and energy dissipation through interfacial friction, increasing at higher V_G (Fig. 3B).

These fibers also show an extraordinary elongation at break ($\varepsilon_{max,\ fiber}$) up to 1.10 (Fig. 3E and fig. S15, B to E), compared with $\varepsilon_{max} = 0.75$ for a monolithic PC film (fig. S15F) (*25*) and higher ultimate strengths of 160 MPa (fiber 1) and 135 MPa (fiber 2), compared with 120 MPa for the PC films (fig. S15F) and fiber (Figs. 3E). A helical telescoping/twisting of the scrolled layers can explain these, which are generally found in natural structural materials to provide higher strength and toughness (*26*). For an Archimedean spiral described by radius r, the cross section follows $r = t\theta$, with t the interlayer distance between successive turnings through the angle θ. The scroll fiber is unique,

requiring that failure traverses the entire path length S_θ of the spiral inclusion (graphene), given by

$$S_\theta = \frac{1}{2}t\left[\theta\sqrt{1+\theta^2} + \ln\left(\theta + \sqrt{1+\theta^2}\right)\right] \quad (2)$$

where S_θ is identically the starting width of the graphene sheet (2.2 cm). For a fiber of diameter 131 ± 3 μm, as in Fig. 1G, Eq. 3 predicts a t of 390 ± 20 nm, in agreement with ellipsometer measurement values of 390 ± 4 nm (table S1). The scroll architecture mandates that all of $m = S_\theta / b_{c\text{-}c}$ (where $b_{c\text{-}c}$ is the carbon-carbon bond length, 0.142 nm) carbon-carbon bonds in the graphene rupture for complete failure or collapse, a process that takes place over a large strain range due to the semi-infinite nature of the graphene herein. This can be seen in the images of the break sites with visible spiral ripping in III to V of Fig. 3D. The spiral geometry predicts that for an initial l (length) × S_θ graphene sheet, the failure strain $\varepsilon_{max,\,fiber}$ is

$$\varepsilon_{max,fiber} = \frac{\sqrt{l^2 + S_\theta^2} - l}{l} + \varepsilon_{max,film} \quad (3)$$

where $\varepsilon_{max,\,film}$ is the failure strain of the planar composite film. For a typical scroll fiber in this work, with l = 2 cm, S_θ = 2.2 cm, and $\varepsilon_{max,\,film}$ = 0.75, we calculate $\varepsilon_{max,\,fiber}$ = 1.24 theoretically, higher than the maximum experimental value of 1.10 (Fig. 3E and fig. S15, B to E).

Last, this approach at the platelet limit offers interesting opportunities to modify the properties of matrices with exceedingly small amounts of an inclusion. PC is transparent but electrically insulating. Graphene electrical continuity was maintained during stacking and folding, as demonstrated by the highly anisotropic electrical conduction in planar 4^j samples at a mere $V_G \approx 0.003\%$ while retaining transparency. Percolation values of 0.14 to 1.3% were reported for various random composites of GO/PC (*15*, *16*, *17*, *27*), for example. A tungsten microprobe (Fig. 4A and fig. S12) inserted perpendicularly to the graphene layer direction at 1.00 μm/s into the grounded composite while maintaining circuit continuity (Fig. 4B) shows discrete current steps as each successive layer is contacted (Fig. 4C), reaching a maximum of about 0.2 μA after the contact of the fourth layer of graphene. Discretized conduction is seen in the all-points histogram in Fig. 4D and fig. S16, with Fig. 4, E and F, showing the scanning electron microscope (SEM) images of the deformation and penetration site with a tapered hole and peripheral diameter = 19.5 ± 0.5 μm. Overall, 4^j composites have anisotropic conduction with σ = 4.17 S/cm in plane at $V_G \approx 0.185\%$, and no continuity orthogonal to alignment, with similar results for scroll fiber composites. This ability to individually address each layer electrically within the composite can allow for complex circuits to be formed therein.

In conclusion, these results highlight new material properties available at this extreme platelet limit for nanocomposites. The 4^j stacking and shear scrolling methods offer straightforward, simple processing steps compared with more complex methods designed to achieve good dispersion at scale (supplementary text 6). The synthesis and transfer of CVD graphene is also advancing rapidly (*28*) with recent increases in scale (*29*). Scrolled fiber architecture promises high elongation at break, strength, and anisotropic conductivity while allowing many different host polymer matrices throughout the interior, distinct from a pure carbon fiber architecture. There exists a substantial opportunity to generate composite materials with new combinations of mechanical reinforcement, electrical, and optical properties at miniscule additions of a semi-infinite nanoplatelet filler.

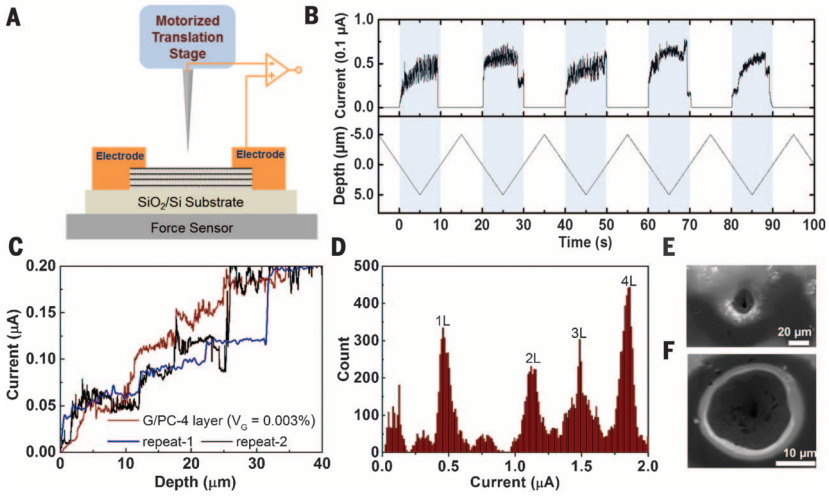

Fig. 4. Electric properties study of the planar composites. (**A**) A microprobe system for simultaneously testing the electrical properties of the G/PC composite; a tungsten microprobe mounted on the motorized translation stage system has a shaft diameter of 80 μm tapering to a 100-nm tip. As the conducting probe contacts each successive layer of graphene, conducting through the probe discretely increases. (**B**) Periodic current cycles formed by the contact and disengagement of the microprobe with G/PC composite surface. The velocity of the microprobe was kept at 1.00 μm/s (down) and –1.00 μm/s (up) alternately with a time span of 10 s and voltage = 1.0 mV. Light blue color areas indicate the contacting durations between the microprobe and the composite surface. (**C**) The electric current curves versus depth trace during the microprobe movement (1.00 μm/s, 1.0 mV) and penetration process for three similar G/PC composite samples ($V_G \approx 0.003\%$, four layers). (**D**) The histogram profiles of the value distribution (count) of electric current signals measured in (C) (red). (**E** and **F**) SEM images of a typical fracture site on the composite film punched by the microprobe; scale bars are 20 and 10 μm, respectively.

REFERENCES AND NOTES

1. J. D. Eshelby, *Proc. R. Soc. London Ser. A* **241**, 376–396 (1957).
2. X. Wang *et al.*, *Mater. Res. Lett.* **1**, 19–25 (2013).
3. Z. Zhou *et al.*, *Carbon* **75**, 307–313 (2014).
4. H. Liu, L. C. Brinson, *Compos. Sci. Technol.* **68**, 1502–1512 (2008).
5. P. M. Ajayan, J. M. Tour, *Nature* **447**, 1066–1068 (2007).
6. C.-W. Nan, Q. Jia, *MRS Bull.* **40**, 719–724 (2015).
7. A. Reina *et al.*, *Nano Lett.* **9**, 30–35 (2009).
8. X. Li *et al.*, *Science* **324**, 1312–1314 (2009).
9. Y.-H. Lee *et al.*, *Adv. Mater.* **24**, 2320–2325 (2012).
10. A. C. Ferrari *et al.*, *Phys. Rev. Lett.* **97**, 187401 (2006).
11. R. R. Nair *et al.*, *Science* **320**, 1308 (2008).
12. C.-J. Shih *et al.*, *Nat. Nanotechnol.* **6**, 439–445 (2011).
13. C. S. Ruiz-Vargas *et al.*, *Nano Lett.* **11**, 2259–2263 (2011).
14. Q.-Y. Lin *et al.*, *ACS Nano* **7**, 1171–1177 (2013).
15. J. R. Potts, S. Murali, Y. Zhu, X. Zhao, R. S. Ruoff, *Macromolecules* **44**, 6488–6495 (2011).
16. P. Steurer, R. Wissert, R. Thomann, R. Mülhaupt, *Macromol. Rapid Commun.* **30**, 316–327 (2009).
17. H. Kim, C. W. Macosko, *Polymer (Guildf.)* **50**, 3797–3809 (2009).
18. B. Shen, W. Zhai, M. Tao, D. Lu, W. Zheng, *Compos. Sci. Technol.* **86**, 109–116 (2013).
19. H. Kim, A. A. Abdala, C. W. Macosko, *Macromolecules* **43**, 6515–6530 (2010).
20. J. R. Potts, D. R. Dreyer, C. W. Bielawski, R. S. Ruoff, *Polymer (Guildf.)* **52**, 5–25 (2011).
21. X. Li, G. B. McKenna, *ACS Macro Lett.* **1**, 388–391 (2012).
22. T. Ramanathan *et al.*, *Nat. Nanotechnol.* **3**, 327–331 (2008).
23. N. A. Koratkar *et al.*, *Appl. Phys. Lett.* **87**, 063102 (2005).
24. J. Meaud *et al.*, *ACS Nano* **8**, 3468–3475 (2014).
25. M. J. Kendall, C. R. Siviour, *Philos. Trans. R. Soc.* **372**, 20130202 (2014).
26. S. E. Naleway, M. M. Porter, J. McKittrick, M. A. Meyers, *Adv. Mater.* **27**, 5455–5476 (2015).
27. M. Yoonessi, J. R. Gaier, *ACS Nano* **4**, 7211–7220 (2010).
28. E. O. Polat *et al.*, *Sci. Rep.* **5**, 16744 (2015).
29. W. Ren, H.-M. Cheng, *Nat. Nanotechnol.* **9**, 726–730 (2014).

ACKNOWLEDGMENTS

This work was primarily funded by 2009 U.S. Office of Naval Research Multidisciplinary University Research Initiatives (MURI) grant on Graphene Approaches to Terahertz Electronics (GATE) at Massachusetts Institute of Technology (MIT), Harvard University, and Boston University. This work was also supported in part by the U.S. Army Research Laboratory (ARL) and the U.S. Army Research Office (ARO) through the Institute for Soldier Nanotechnologies (ISN), under contract number W911NF-13-D-0001. R.L. is supported by a NASA Space Technology Research Fellowship (NSTRF), and B.Q. is supported by a National Defense Science and Engineering Graduate (NDSEG) Fellowship. We appreciate characterization support from the ISN at MIT funded by U.S. ARO and MIT Department of Materials Science and Engineering NanoLab. We also thank A. Schwartzman (MIT NanoLab) for the microindentation and uniaxial tensile test of 4^j samples; P. Moy and V. Wu of ARL for the imaging of the scrolled fibers in the tensile test; and E. Cohen for careful review of the manuscript and differential scanning calorimetry/dynamic mechanical analysis data.

SUPPLEMENTARY MATERIALS

www.sciencemag.org/content/353/6297/364/suppl/DC1
Materials and Methods
Supplementary Text
Figs. S1 to S18
Table S1
References (*30*–*59*)

7 February 2016; accepted 21 June 2016
10.1126/science.aaf4362

Layered and scrolled nanocomposites with aligned semi-infinite graphene inclusions at the platelet limit

Pingwei Liu, Zhong Jin, Georgios Katsukis, Lee William Drahushuk, Steven Shimizu, Chih-Jen Shih, Eric D. Wetzel, Joshua K. Taggart-Scarff, Bo Qing, Krystyn J. Van Vliet, Richard Li, Brian L. Wardle and Michael S. Strano

Science **353** (6297), 364-367.
DOI: 10.1126/science.aaf4362

Stacking up the filler material

In composite materials, a strong or stiff filler is added to a softer matrix to create a combined material with better mechanical or electrical properties. To minimize the filler content, it needs to be uniformly distributed in the composite, which is particularly challenging for nanoscale materials. Liu *et al.* alternately stacked sheets of graphene and polycarbonate to make a base composite. By further cutting and stacking, up to 320 aligned layers were made with a very uniform filler distribution. Alternatively, the initial stack could be rolled into a rod. In both cases, the properties exceeded what might be expected from a simple combination of the two materials.

Science, this issue p. 364